ISSN 1023-1935, Russian Journal of Electrochemistry, 2019, Vol. 55, No. 4, pp. 272–280. © Pleiades Publishing, Ltd., 2019.
Published in Russian in Elektrokhimiya, 2019, Vol. 55, No. 4, pp. 414–423.

Study of the Corrosion Resistance Properties of Ni–P and Ni–P–C Nanocomposite Coatings in 3.5 wt % NaCl Solution[1]

Ramin Badrnezhad[a], Hamed Pourfarzad[b, *], Ali Reza Madram[c], and Mohammad Reza Ganjali[b, c]

[a] *Department of Chemistry and Chemical Engineering, Malek-Ashtar University of Technology, Tehran, 15875-1774 Iran*
[b] *Center of Excellence in Electrochemistry, Faculty of Chemistry, University of Tehran, Tehran, 14155-6455 Iran*
[c] *Endocrinology and Metabolism Research Center, Tehran University of Medical Sciences, Tehran, 14155-6455 Iran*
**e-mail: h.pourfarzad2030@gmail.com*

Received January 6, 2017; revised June 30, 2017; accepted October 16, 2017

Abstract—The present paper aims to compare the corrosion protection performance of electrodeposited Ni–P with Ni–P–C nanocomposite coatings in 3.5 wt % NaCl solution in order to assess the influence of carbon nanoparticles on corrosion behavior of these coatings, by the potentiodynamic polarisation Tafel curves and electrochemical impedance spectroscopic (EIS) techniques. The effect of heat treatment on the coatings performance was also studied. The results revealed that heat treated Ni–P–C nanocomposite coating in air at 673 K significantly improved resistance to corrosion compared with Ni–P coatings. This behavior was related to incorporation of carbon nanoparticles into Ni–P matrix using in-situ electrochemical reduction of *L*-lysine, which shift the corrosion potential (E_{corr}) positively, also the corrosion current density (I_{corr}) and the double layer capacitance (C_{dl}) values decrease, the charge transfer resistance (R_{ct}) and efficiencies of inhibition (IE, %) increase, indicating improvement in the corrosion resistance in seawater environment. Microstructure, phase change and chemical composition of the prepared coatings were studied using scanning electron microscopy (SEM), X-ray diffraction (XRD) and elemental microanalysis (EDX), respectively.

Keywords: corrosion protection, carbon nanoparticles, Ni–P–C nanocomposite coating, electrochemical impedance spectroscopy, electrodeposited coatings

DOI: 10.1134/S1023193519030029

INTRODUCTION

Electrodeposited composite coatings based on a Ni–P alloy matrix containing different fine particles of nonmetallic, ceramic or polymer compounds [1–10] have attracted attention in many industrial fields due to their good mechanical, chemical and electrocatalytic properties including enhanced wear resistance combined with a good corrosion resistance and especially high electrocatalytic activity for hydrogen evolution reaction (HER) in chlor-alkali industries and water electrolysis [11–17], when compared to pure nickel coatings.

Ni–P coating with phosphorus content over 9 wt % are considered amorphous and possesses excellent mechanical properties such as corrosion resistance [18, 19]. This protective film can be deposited by electroplating and electroless plating onto a metallic or nonmetallic substrate to prevent attack by hostile environments [20]. Electrolytic Ni–P systems are favored over chemical (electroless) deposition systems, since electrolytic process routes are providing higher deposition rates, enhanced electrolyte stability and in case of dispersion coatings a more precise control of particle incorporation.

Ni–P coatings are important engineering materials and demonstrated high intrinsic electrocatalytic activity in HER and exhibited better catalytic capability than single Ni catalyst and in addition to cost effective than electrocatalysts based on noble metals, because of synergistic electronic effect among alloys [21–24].

The traditional water electrolysis in alkaline media by hydrogen evolution reaction (HER), has received wide attention because of its important in both fundamental and technological electrochemistry, supplies a non-polluting method of hydrogen production although it is not the cheapest method of hydrogen production. Therefore, low-cost production of hydrogen is a key factor for bringing this technology to commercialization [25–27]. In the other side, water is most often found in nature as seawater (about 98%) and seawater is a natural electrolyte. Unlike most other water sources, seawater in the world's oceans has a salinity of about 3.5 wt %. Thus, seawater electrolysis is one of the promising ways to produce hydrogen because first, it is available in plentiful supply on the earth and second, the seawaves-generated power and

[1] The article is published in the original.

Table 1. Composition and operating conditions of the plating baths

Constituents and operating conditions of plating baths	Bath		
	A	B	C
Nickel sulfate, M	1.14	1.14	1.14
Nickel cloride, M	0.19	0.19	0.19
Boric acid, M	0.49	0.49	0.49
Sodium citrate, M	0.12	0.12	0.12
Sodium hypophosphite, M	–	0.14	0.14
L-lysine, M	–	–	0.06
Applied current, mA cm^{-2}	22	22	13
Time, min	30	45	45
Temperature, K	298	298	298
Total thickness of deposit, μm	21–22	35–37	46–47

its utilization in situ for the hydrogen generation by seawater electrolysis is a very interesting way [28].

The electrode materials with high catalytic activity for the hydrogen evolution reaction (HER) should have characteristics such as: large active surface area, low cost, ease of use, and especially must have electrochemical stability and high corrosion resistance. In our previous work, we found that nickel–phosphor–carbon (Ni–P–C) nanocomposite coatings prepared by co-electrodeposition of Ni–P with carbon from *L*-lysine source, benefit of good catalytic activity for the HER, in which the observed activity was mainly due to the intrinsic activity induced by carbon embedded into Ni–P matrix [29].

The electrochemical stability and the corrosion resistance of the electrode materials for long operation time are important for their industrial applications [14, 30]. For this reason, corrosion behavior have to be considered at an appropriate stage of material development for hydrogen production by seawater electrolysis.

This paper presents the first attempt to investigate the effect of incorporation of carbon nanoparticles via electrochemical reduction of *L*-lysine amino acid source on the nanostructure and anti-corrosion properties of the as-deposited electrodeposited Ni–P, Ni–P–C matrix over long time periods in seawater aggressive chloride environment (3.5 wt % NaCl solution) by with emphasis on surface morphology, chemistry, phase content and heat treatment on corrosion resistance, using potentiodynamic polarization and electrochemical impedance spectroscopy (EIS) methods.

EXPERIMENTAL

Materials and Coatings

Ni–P and Ni–P–C composite coatings were electrochemically and under galvanostatic conditions deposited from baths (A and B) and (A, B and C), in two and three-step method, respectively. A copper electrode sealed in a heat shrinkable tube exposing a 2.5 cm^2 surface area as substrate, and a platinum plate (99.99% Pt) with more than 25 cm^2 as counter electrode. Before electrodeposition, the copper substrate was polished with sandpaper (P 600, Siawats), washed with water, immersed in a 1 : 1 HNO_3, washed with water, and immediately introduced into the two compartment Pyrex® glass cell for electrodeposition. Composition of the baths and electrodeposition conditions of each step are given in Table 1. All chemicals were of analytical reagent grade, Merck company and were used as received.

Surface morphology and elemental composition of the alloys were investigated by scanning electron microscopy (SEM) and energy dispersive X-ray diffraction microanalysis (EDX) (Philips-XL-30). Crystal structure of the alloys was determined by X-ray diffraction (XRD) analysis (Philips-X'Pert-MPD) using CuK_α wavelength of 1.5418 Å. To confirm the phase-change in Ni–P–C nanocomposites the differential scanning calorimetry method (DSC) was used (Setaram-SETSYS Evolution DTA/DSC).

A three-electrode open cell with Ni–P and Ni–P–C *L*-lysine composite coatings as working electrode (WE), a large surface area Pt plate (25 cm^2, Pt 99.99%) as counter electrode (CE) and Ag/AgCl as reference electrode (RE) mounted for electrochemical measurements. All measurements were performed in purified 3.5 wt % NaCl solution degassed with argon gas (99.99%) at 298 K. Before each experiment the cell was washed with hot water H_2SO_4, NaOH, many times with hot distilled water, and finally with 3.5 wt % NaCl, and kept under argon atmosphere until used.

The steady-state potentiodynamic polarization Tafel curves were made at a scan rate of 1 mV/s in the applied potential range from (–625 mV, Ag/AgCl) to (+240 mV, Ag/AgCl) respect to E_{corr}. The polarization curves were recorded after a month of immersion.

The EIS measurements were performed at the steady-state. A 10 mV amplitude AC potential superimposed on a DC potential was applied, and a wide

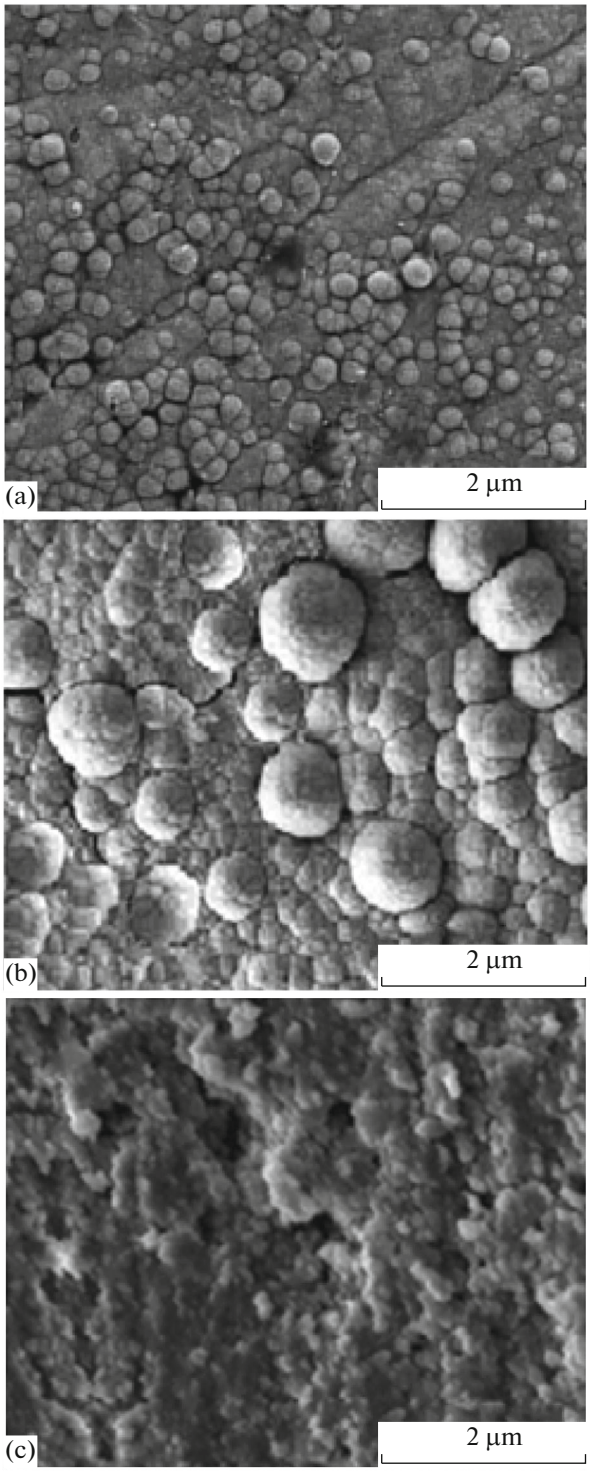

Fig. 1. The SEM images of (a) as deposited $Ni_{83}P_{17}$ (b) as-deposited $Ni_{81}P_{16}C_3$ and (c) heated $Ni_{81}P_{16}C_3$ in air at 673 K composite electrodes.

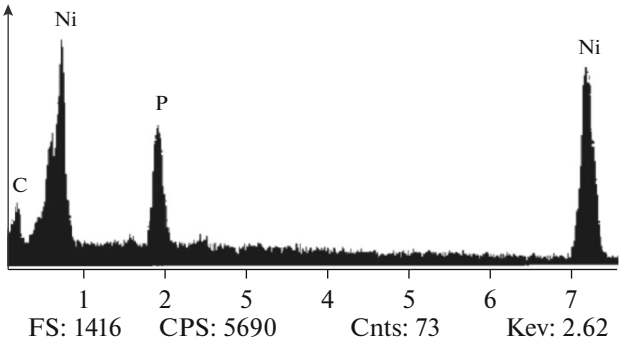

Fig. 2. Energy dispersive X-ray diffraction (EDX) micro-analysis spectrum of as-deposited $Ni_{81}P_{16}C_3$ coating.

range of the frequency, 100 kHz to 0.001 Hz, was scanned with thirty points per decade in logarithmic scale, and the impedances as well as current potential phase angles were recorded. In order to obtain the stationary conditions necessary for impedance measurements, the working electrodes were polarized at 100 mA for 2 h in 3.5 wt % NaCl solution at 25°C.

Measurements were performed by using an Potentiostat/Galvanostat EG&G2273A and Frequency Response Analyzer 1025 EG&G controlled by GPIBIEEE-NI-488II. The Tafel curves and EIS data acquisition were carried out using a Labviews subroutine and EG&GPowerSine softwares, respectively, and EIS data approximated using ZView software and the modified complex nonlinear least square (CNLS) method.

RESULTS AND DISCUSSION

Surface Morphology and Composition of Coatings

SEM micrographs obtained on the surface of as-deposited Ni–P (Fig. 1a) and as deposited Ni–P–C (Fig. 1b) heated Ni–P–C composite coatings (Fig. 1c) displayed globular fungi-form characters that were deformed upon heating of the coating at 673 K in air atmosphere (Fig. 1c). A minimum diameter of 30 nm was observed for globular fungi-form characters in the SEM micrograph.

A typical EDX spectrum obtained from the surface of as-deposited Ni–P–C coating is presented in Fig. 2. Similar patterns were observed for heated coating implying that carbon content of composite does not alter upon heat treatment. Chemical composition of the top layers of the coatings prepared under optimized conditions were $Ni_{83}P_{17}$ (as-deposited and heated), and $Ni_{81}P_{16}C_3$ (as-deposited and heated). These results proves incorporation of carbon in Ni–P matrix and are similar to those reported by Wu et al. [31] for Ni–P–C (graphite) electrode.

Crystallization and Structure of Composite Coatings

The diffraction patterns of studied coatings are shown in Fig. 3 for as-deposited (a) and heated (b) composite coatings. It is observed that the as-depos-

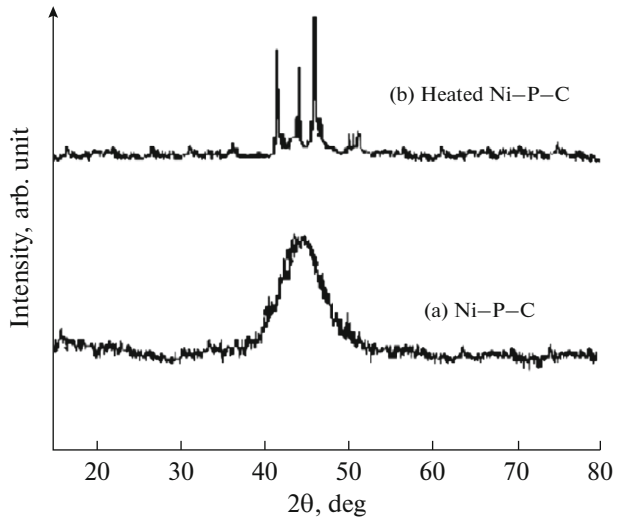

Fig. 3. XRD spectra of as-deposited (a) and heated in air at 673 K (b) $Ni_{81}P_{16}C_3$ electrodes using CuK_α wavelength of 1.5418 Å.

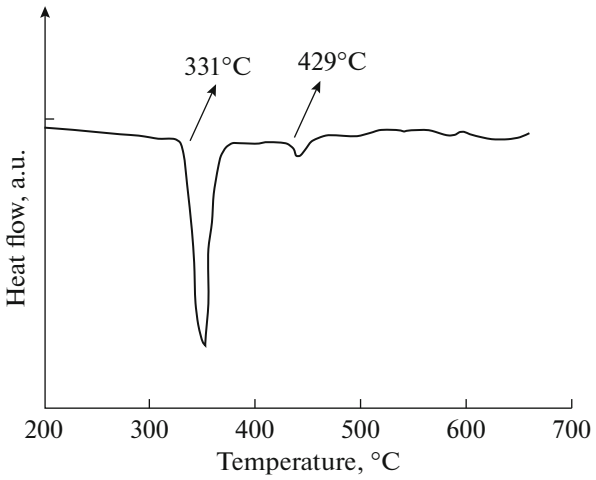

Fig. 4. Differential scanning calorimetry curve for $Ni_{81}P_{16}C_3$ electrodes using temperature range from 473 to 973 K in air atmosphere.

ited coatings had amorphous Ni–P–C structure and exhibited a single broad peak centered at 44.5°, and changed into crystalline form after heat treatment at 673 K for 1 h, as a result of transformation of Ni–P matrix to the system comprising nickel and nickel phosphide (Ni_3P) as dominant phases at 673 K [31]. It seems that carbon particles have been dispersed in nickel and nickel phosphide phases, and formed $Ni_{81}P_{16}C_3$ nanocomposite coating. The XRD patterns obtained here for Ni–P–C composite coatings prepared via *L*-lysine method by electrodeposition are very similar to those prepared via graphite method by electroless-deposition [31], confirming formation of Ni–P–C composite coatings in this work. As an approximation, Scherrer's equation was used to calculate average grain size. The average grain size was about 78, and 37 nm for $Ni_{83}P_{17}$, and $Ni_{81}P_{16}C_3$, respectively. Clearly, addition of carbon into the Ni–P matrix has decreased average of the grain size. Similar behavior has been reported by Meguro et al. [32, 33].

For full approval the phase-change in Ni–P–C nanocomposites that were under heat treatment at 673 K temperature the differential scanning calorimetry method (DSC) was used. As can be seen in Fig. 4 an identified and single exothermic peak exists in the studied temperature regions with an initial temperature 331°C that is related to phase change from amorphous to crystalline structure. A similar behavior has been reported for Ni–P amorphous alloys [31]. It should be noted at temperatures below 200°C, there is no specific changes and therefore not shown in Fig. 4.

KINETIC STUDIES

Potentiodynamic Polarisation Studies

The potentiodynamic polarisation behaviour of as deposited Ni–P alloy and Ni–P–C coatings in deaerated 3.5 wt % NaCl solution are shown in Fig. 5. As seen the cathode reaction in the polarization curves corresponded to the evolution of the hydrogen, and the anodic polarization curve was the most important features related to the corrosion resistance [34].

In corrosion, quantitative information on corrosion currents and corrosion potentials can be extracted from the slope of the curves, also polarization resistance values will determine using the Stern–Geary equation, In the other hand Close to the open circuit corrosion potential, it is expected that the Stern–Geary relationship [35] may be applied. It implicitly considers that both the anodic and cathodic processes are purely additives and that both of them follow the

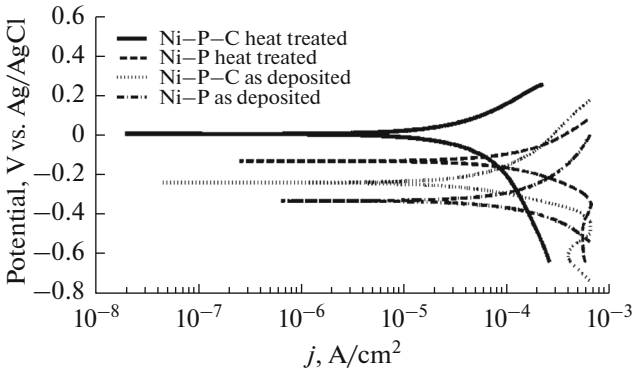

Fig. 5. Steady-state polarization Tafel curves obtained in 3.5 wt % NaCl at 298 K on investigated coatings.

Table 2. Corrosion parameters of the coatings derived from steady state Tafel plots

Type of coatings	E_{corr}, mV	I_{corr}, mA cm^{-2}	R_p, Ohm cm^2	Electrochemical CR[a], mil/year $\times 10^6$	IE[b], %
Ni–P (as deposited)	−342	0.91	202.01	16.60	59.27
Ni–P–C (as deposited)	−239	0.49	307.92	9.02	77.85
Ni–P (heat treated)	−134	0.16	632.79	3.03	92.56
Ni–P–C (heat treated)	+3.32	0.04	7550.98	0.79	98.04

[a] Corrosion rate.
[b] Corrosion inhibition efficiency.

Tafel law. The global current density can then be expressed by the following equation:

$$I = I_{corr} \times \{\exp[\beta a(E - E_{corr})] - \exp[\beta c(E - E_{corr})]\}. \quad (1)$$

With apply a small signal approximation to above equation, the following Stern–Geary equation is obtained [36]:

$$I_{corr} = \frac{1}{2.303R_p}\left(\frac{\beta_a\beta_c}{\beta_a + \beta_c}\right). \quad (2)$$

• I_{corr} is the corrosion current density in A/cm^2; was determined by extrapolating the straight-line section of the anodic and cathodic Tafel lines;

• R_p is the corrosion resistance in Ohm cm^2;

• β_a is the anodic Tafel slope in V/decade or mV/decade of current density;

• β_c is the cathodic Tafel slope in V/decade or mV/decade of current density;

• the quantity, $(\beta_a\beta_c)/(\beta_a + \beta_c)$, is referred to as the Tafel constant.

The corrosion potential (E_{corr}), corrosion current density (I_{corr}) and polarization resistance (R_p), which were obtained from the potentiodynamic polarization curves are summarized in Table 2.

Also corrosion rates (CR) were calculated by the Faraday law as follows [37]:

$$\mathrm{CR\,(mil/year)} = \frac{0.13I_{corr}(\mathrm{Eq.\ wt})}{d}, \quad (3)$$

where Eq. wt is the equivalent weight and d is the density of the Nickel metal in g/cm^3.

Also corrosion current density (I_{corr}) were used to calculate the corrosion inhibition efficiency (IE, %) of the coatings according to following relationship:

$$\mathrm{IE\,(\%)} = \left(\left(1 - \frac{I_{corr}(\mathrm{i})}{I_{corr}(\mathrm{o})}\right) \times 100\right), \quad (4)$$

where I_{corr}(i) and I_{corr}(o) are the corrosion current densities for the composite coatings and the substrate, respectively.

Comparison of the electrochemical parameters (Table 2) of the as deposited Ni–P and Ni–P–C composite coatings reveal that E_{corr} shifted towards the noble (positive) direction, I_{corr} values decreased and R_p increased with the incorporation of carbon particles in the matrix, indicating better corrosion protective properties of the coatings. In other words, the Ni–P–C nanocomposites possess better chemical stability in seawater environment also helps to prevent the corrosive pits from growing up and contributes to accelerate the passivation process of the metal matrix as well.

$\log(i)$–E curves for the Ni–P and Ni–P–C deposits with an heat treatment in air atmosphere at 673 K for 1 h are shown in Fig. 5. The corrosion potential E_{corr} of the heat treated Ni–P and Ni–P–C deposits is positively shifted and also I_{corr}, which reflects the corrosion rate of the heated coatings become distinctly smaller compared to as plated deposits. Therefore, the high corrosion resistance of heated Ni–P and Ni–P–C coating is expected, which could effectively extend the application of them.

The above results are attributable to the following reasons. First, the phase transformation of a Ni–P deposit from the amorphous solid phase to the crystalline structure occurs at 673 K since the crystallization of a Ni–P deposit with a supersaturated P content and thus formation of crystalline phases of nickel and nickel phosphide with remarkable thermodynamic stability. Second the annealing treatment also favors the movement of surface Ni and P atoms, as a consequence the amount of free nickel and phosphour is reduced, resulting in the formation of compact, smooth and homogenous deposits, which was found from the SEM observation. Third the corrosion potential of the heated deposits positively moved due to the formation of Ni oxide on the surface of deposits since the surface P has been found to be replaced by oxygen species from the air after the heat treatment. In fact, the main purpose of the heat treatment in air is to form a uniform film consisting of Ni–P and NiO on the deposit surface, increasing the anticorrosive ability of Ni–P deposits [38].

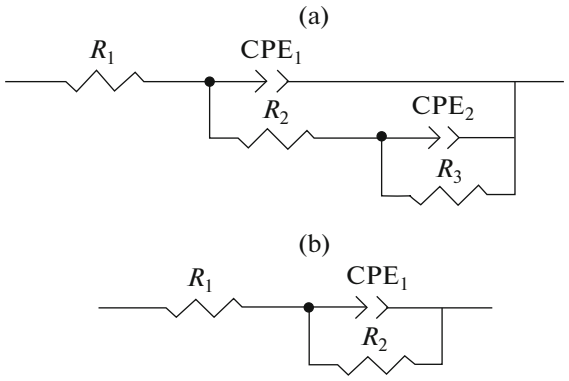

R_1 Resistance of solution
R_2 Coating resistance
R_3 Corrosion resistance
CPE_{dl} Constant phase element

Fig. 6. Randles equivalent electrical circuit model used to analyze the EIS spectra, (a) equivalent circuit for Ni–P–C heated composite coating, (b) equivalent circuit for Ni–P coatings and Ni–P–C as deposited coating.

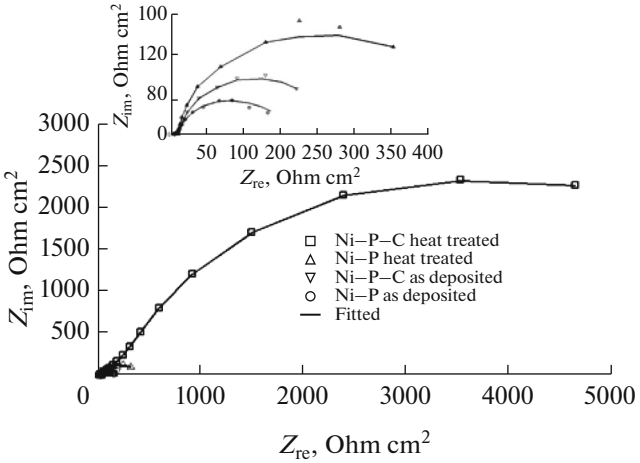

Fig. 7. Nyquist plots of Ni–P and Ni–P–C coatings in 3.5 wt % NaCl.

Electrochemical Impedance Spectroscopy Studies

EIS is a non-destructive and powerful technique capable of providing information about all resistive, capacitive, and inductive contributors in short period of time using appropriate equivalent circuit mode (Fig. 6). Hence, this technique allows several electrochemical parameters can be evaluated and interfacial relaxations such as corrosion phenomena and adsorption behavior of thin films can be detected [39, 40].

Figure 7 shows the Nyquist plots from the EIS measurements for the Ni–P and Ni–P–C composite coatings in 3.5 wt % NaCl solution at their respective E_{corr}. It is clear that the obtained diagrams for Ni–P coatings and Ni–P–C as deposited coating show a single semi circle and one capacitive loop in the whole investigated frequency range (suggesting an activation mechanism for the corrosion process). Whereas for the Ni–P–C thermally treated coating it is characterized by presence of two semicircles of different diameter in the Nyquist plots in the investigated frequency range indicated the presence of two time constants.

The diameter of the second semicircle decides the corrosion resistance of the coatings. The semicircle at the higher frequency region is related to the bulk reactions and the following semicircle at the lower frequency region is related to the coating/solution interface.

From the Nyquist plot it also can be seen that the Ni–P–C heated composite coating exhibits the biggest radius compared with the other coatings, indicating that the Ni–P–C heat treated nanocomposite exhibits better corrosion resistance compared with the other coatings [41, 42] and the previous Ni–P coatings [43]. Because Ni–P–C heated is free of phase boundaries and the absence of the defects in crystalline nanocomposites such as stacking faults and segregation, and carbon nanoparticles are capable of filling some of the pores in the coating and prevent further diffusion of corrosive species along the interface.

The appearance of a single inflection point and a single phase angle maximum in the Bode plots obtained for Ni–P coatings and Ni–P–C as deposited coating Figs. 8, 9, indicate that the process involves only a single time constant. This result is in accordance with the reports of the other authors [44–46]. Also Bode plots obtained for Ni–P–C heated composite coating gave two inflection point and two peaks (phase angle vs. frequency) at investigated frequency range which clearly indicate the presence of two time constants.

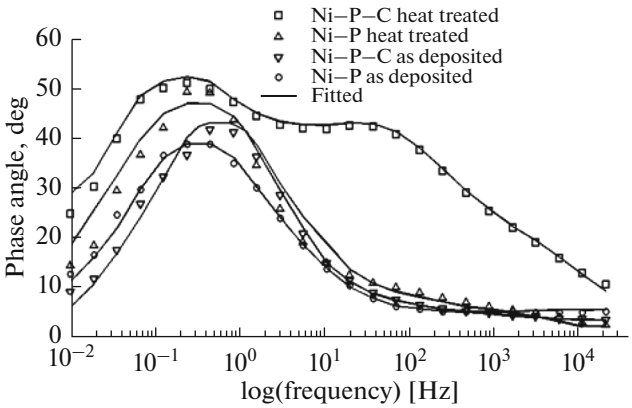

Fig. 8. Bode phase plots of Ni–P and Ni–P–C coatings in 3.5 wt % NaCl.

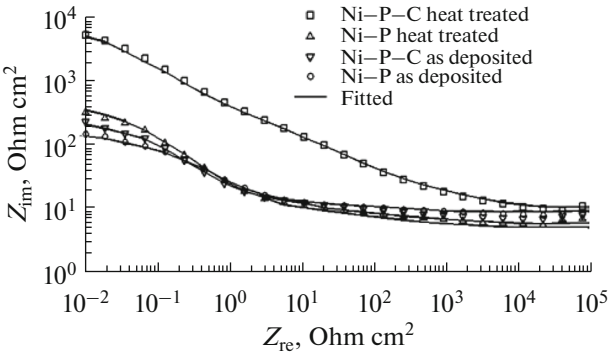

Fig. 9. Bode phase plots of Ni–P and Ni–P–C coatings in 3.5 wt % NaCl.

Figure 9 shows that the increase of absolute impedance at low frequencies in the Bode plot confirms the higher protection with incorporation of carbon nanoparticles in the coatings.

As a result of an approximation of the experimental data using the designed one and two CPE model, the following parameters could be obtained: R_p, R_s, T, ϕ, where T is the capacity parameter and ϕ is a dimensionless dispersion parameter related to CPE model (the value of ϕ changes between zero to one, and is equal to one for complete smooth electrode, i.e. for $\phi = 1$, $T = C_{dl}$). $Z_{CPE} = 1/[(j\omega)^{\phi}T]$, where ω is the angular frequency of ac voltage. The double-layer capacitance C_{dl} was calculated according to [47]:

$$T = C_{dl}^{\phi}\left(\frac{1}{R_s}+\frac{1}{R_p}\right)^{1-\phi}. \quad (5)$$

The R_{ct} and C_{dl} values of composite coatings, are reported in Table 3. The R_{ct} of Ni–P (as-deposited), Ni–P–C (as-deposited), Ni–P (heat treated) and Ni–P–C (heat treated) composite coating, are 226, 482, 738.8 and 9655 Ohm cm^2, respectively and the corresponding C_{dl} values are (0.54), (0.36), (0.15) and (0.01) mF cm^{-2}, respectively. It has been established that high values of R_{ct} and low values of C_{dl} imply better corrosion protective ability of coatings [48, 49].

The ratio of the value of capacitance C_{dl} to the capacitance of an ideal smooth surface of electrolytic nickel (20 μF cm^{-2} [47]) gives a value of surface roughness factor, R_f. This value for the Ni–P–C thermally treated coatings is about forty times lower than for the Ni–P–C as-deposited coatings, indicating more efficient blocking of the corrosion process. Further evidence for this is the higher value of the polarization resistance R_p for the treated coatings, than for the as-deposited coatings (Table 2).

The EIS results also consistent with the results of the potentiodynamic polarisation technique in 3.5 wt % NaCl solution and confirm that the Ni–P–C composite coatings as a catalyst for HER have the significant anti-corrosion performance.

CONCLUSIONS

In summary, the following conclusions have been drawn from the present investigation:

(1) The inclusion of carbon particles in Ni–P binary alloy matrix was achieved successfully via *L*-lysine reduction during electrodeposition from an electroplating bath. The carbon particles appear well dispersed in the nickel-phosphur coating and covered the surface of the coating. The related corrosion parameters showed that the incorporation of carbon particles from amino acid *L*-lysine carbon source into the nickel-phosphur coating significantly increased the corrosion resistance. Because, the carbon particles uniformly distributed in the nickel–phosphur coating and increased corrosion potential of the formed nanocomposite coating towards more positive values, restricting localized corrosion, and result in mainly homogenous corrosion.

(2) Electrochemical measurements showed that Ni–P–C *L*-lysine coatings after thermal treatment are more resistant to corrosion in 3.5 wt % NaCl solution than in the as-deposited condition. A more positive value of the corrosion potential, a lower value of the corrosion current and surface roughness factor and also a higher value of the polarization resistance is observed for the thermally treated coating at 673 K temperature. The reason for this is presence of crystalline

Table 3. Data obtained from the EIS spectra simulation

Type of coatings	R_s, Ohm cm^2 [a]	R_{ct}, Ohm cm^2 [b]	C_{dl}, mF/cm^2 [c]	R_f [d]
Ni–P (as-deposited)	7.75	226	0.54	26.78
Ni–P–C (as-deposited)	8.06	482	0.36	18.24
Ni–P (heat treated)	9.97	739	0.15	7.33
Ni–P–C (heat treated)	10.08	**9655**	0.01	0.54

[a] Solution resistance.
[b] Charge transfer resistance.
[c] Double layer capacitance.
[d] Roughness factor.

phases of nickel and nickel phosphide with remarkable thermodynamic stability. Moreover, parameters determined by the EIS method provide a means for estimating the corrosion resistance of coatings, and confirm the results obtained from potentiodynamic measurements.

FUNDING

The authors thank to excellence center in electrochemistry for providing the facilities to bring about this work, and also Malek-Ashtar university of Technology for providing financial support by Major Research Project.

REFERENCES

1. Berkh, O., Bodnevas, A., and Zahavi, J., Electrodeposited Ni–P–SiC composite coatings, *Plat. Surf. Finish,* 1995, vol. 82, pp. 62–66.
2. Sharma, S.B., Agarwala, R.C., Agarwala, V., and Ray, S., Dry sliding wear and friction behavior of Ni–P–$ZrO_2Al_2O_3$ composite electroless coatings on aluminum, *Mater. Manuf. Processes,* 2002, vol. 17, pp. 637–649.
3. Aghaie, E., Najafi, A., Maleki-Ghaleh, H., and Mohebi, H., Effect of SiC concentration in electrolyte on Ni–SiC composite coating properties, *Surf. Eng.,* 2013, vol. 29, pp. 177–182.
4. Chen, W., Gao, W., and He, Y., A novel electroless plating of Ni–P–TiO_2 nano-composite coatings, *Surf. Coat. Technol.,* 2010, vol. 204, pp. 2493–2498.
5. Liu, B., Liu, L.R., and Liu, X.J., Effects of carbon nanotubes on hardness and internal stress in Ni–P coatings, *Surf. Eng.,* 2013, vol. 29, pp. 507–510.
6. Alirezaei, S., Monirvaghefi, S.M., Salehi, M., and Saatchi, A., Wear behavior of Ni–P and Ni–P–Al_2O_3 electroless coatings, *Wear,* 2007, vol. 262, pp. 978–985.
7. Farzaneh, A., Mohammadi, M., Ehteshamzadeh, M., and Mohammadi, F., Electrochemical and structural properties of electroless Ni–P–SiC nanocomposite coatings, *Appl. Surf. Sci.,* 2013, vol. 276, pp. 697–704.
8. Sharma, A. and Singh, A.K., Electroless Ni–P–PTFe-Al_2O_3 dispersion nanocomposite coating for corrosion and wear resistance, *J. Mater. Eng. Perform.,* 2014, vol. 23, pp. 142–151.
9. Liu Jianggao, Wang Shubin, Li Pengyang, Feng Mengjie, and Yang Xinwang, A modified dip-coating method to prepare BN coating on SiC fiber by introducing the sol-gel process, *Surf. Coat. Technol.,* 2016, vol. 286, pp. 57–63.
10. Rossi, S., Chini, F., Straffelini, G., Bonora, P.L., Moschini, R., and Stampali, A., Corrosion protection properties of electroless Nickel/PTFE, Phosphate/MoS_2 and Bronze/PTFE coatings applied to improve the wear resistance of carbon steel, *Surf. Coat. Technol.,* 2003, vol. 173, pp. 235–242.
11. Paseka, I., Influence of hydrogen absorption in amorphous Ni–P electrodes on double layer capacitance and charge transfer coefficient of hydrogen evolution reaction, *Electrochim. Acta,* 1999, vol. 44, pp. 4551–4558.
12. Burchardt, T., The hydrogen evolution reaction on NiP_x alloys, *Int. J. Hydrogen Energy,* 2000, vol. 25, p. 627.
13. Burchardt, T., Hydrogen evolution on NiP_x alloys: the influence of sorbed hydrogen, *Int. J. Hydrogen Energy,* 2001, vol. 26, pp. 1193–1198.
14. Popczyk, M., Budniok, A., and Lasia, A., Electrochemical properties of Ni–P electrode materials modified with nickel oxide and metallic cobalt powders, *Int. J. Hydrogen Energy,* 2005, vol. 30, pp. 265–271.
15. Burchardt, T., Hansen, V., and Valand, T., Microstructure catalytic activity towards the hydrogen evolution reaction of electrodeposited NiP_x alloys, *Electrochim. Acta,* 2001, vol. 46, pp. 2761–2766.
16. Krolikowski, A. and Wiecko, A., Impedance studies of hydrogen evolution on Ni–P alloys, *Electrochim. Acta,* 2002, vol. 47, pp. 2065–2069.
17. Shibli, S.M.A. and Dilimon, V.S., Effect of phosphorous content and TiO_2-reinfocement on Ni–P electroless plates for hydrogen evolution reaction, *Int. J. Hydrogen Energy,* 2007, vol. 32, pp. 1694–1700.
18. Bredael, E., Blanpain, B., Celis, J.P., and Roos, J.R., On the amorphous and crystallinestate of electrodeposited nickel-phosphorous coatings, *J. Electrochem. Soc.,* 1994, vol. 141, pp. 294–299.
19. Daly, B.P. and Barry, F.J., Electrochemical nickel-phosphorous alloy formation, *Int. Mater. Rev.,* 2003, vol. 48, pp. 326–338.
20. Lee, H.B., Wuu, D.S., Lee, C.Y., and Lin, C.S., Study of the corrosion behavior of nanocrystalline Ni–P electrodeposited coating, *Metall. Mater. Trans. A,* 2010, vol. 41, pp. 450–459.
21. Cordeiro, G., Mattos, O.R., Barcia, O.E., Beaunier, L., Deslouis, C., and Tribollet, B., Anodic dissolution of nickel in concentrated sulfuric acidic solutions, *J. Appl. Electrochem.,* 1996, vol. 26, pp. 1083–1092.
22. Barbosa, M.R., Bastos, J.A., Garca, J.J., and Vicente, F., Chloride role in the surface of nickel electrode, *J. Electrochim. Acta,* 1998, vol. 44, pp. 957–865.
23. Seyeux, A., Maurice, V., Klein, L.H., and Marcus, P., Initiation of localized corrosion at the nanoscale by competitive dissolution and passivation of nickel surfaces, *J. Electrochim. Acta,* 2008, vol. 54, pp. 540–544.
24. Sun, F., Meng, G., Zhang, T., Shao, Y., Wang, F., and Dong, C., Electrochemical corrosion behavior of nickel coating with high density nano-scale twins (NT) in solution with Cl^-, *J. Electrochim. Acta,* 2009, vol. 54, pp. 1578–1583.
25. Selembo, P.A., Merrill, M.D., and Logan, B.E., The use of stainless steel and nickel alloys as low-cost cathodes in microbial electrolysis cells, *Power Sources,* 2009, vol. 190, pp. 271–278.
26. Grant, J.C., *Nickel.Cadmium Battery Application Engineering Handbook,* 3rd ed., Gainesville: General Electric Company, 1975.
27. Ahn, K.H., Song, K.G., Cha, H.Y., and Yeom, I.T., Removal of ions in nickel electroplating rinse water using low-pressure nanofiltration, *J. Desal.,* 1999, vol. 122, pp. 77–84.

28. Mathu, J., Agarwal, N., Swaroop, R., and Shah, N., Economics of producing hydrogen as transportation fuel using offshore wind energy systems, *Energy Policy,* 2008, vol. 36, pp. 1212–1215.
29. Shervedani, R.K. and Madram, A.R., Electrocatalytic activities of nanocomposite $Ni_{81}P_{16}C_3$ electrode for hydrogen evolution reaction in alkaline solution by electrochemical impedance spectroscopy, *Int. J. Hydrogen Energy,* 2008, vol. 33, pp. 2468–2476.
30. Madram, A.R., Pourfarzad, H., and Zare, H.R., Study of the corrosion behavior of electrodeposited Ni–P and Ni–P–C nanocomposite coatings in 1 M NaOH, *J. Electrochim. Acta,* 2012, vol. 85, pp. 263–267.
31. Wu, Y.T., Lei, L., Shen, B., and Hu, W.B., Investigation in electroless Ni–P–Cg(graphite)–SiC composite coating, *Surf. Coat. Technol.,* 2006, vol. 201, pp. 441–445.
32. Meguro, S., Sasaki, T., Katagiri, H., Habazaki, H., and Kawashima, A., Electrodeposited Ni–Fe–C cathodes for hydrogen evolution articles, *J. Electrochem. Soc.,* 2000, vol. 147, pp. 3003–3309.
33. Hashimoto, K., Sasaki, T., Meguro, S., and Asami, K., Nanocrystalline electrodeposited Ni–Mo–C cathodes for hydrogen production, *J. Mater Sci Eng.,* 2004, vol. 375, pp. 942–945.
34. Dong, H., Sun, Y., and Bell, T., Enhanced corrosion resistance of duplex coatings, *Surf. Coat. Technol.,* 1997, vol. 90, pp. 91–101.
35. Shervedani, R.K. and Lasia, A., Study of the hydrogen evolution reaction on Ni–Mo–P electrodes in alkaline solutions, *J. Electrochem. Soc.,* 1998, vol. 145, pp. 2219–2225.
36. Stern, M. and Geary, A., The mechanism of passivating-type inhibitors TECHNICAL PAPERS, *J. Electrochem. Soc.,* 1958, vol. 105, pp. 638–647.
37. Mishra, R. and Balasubramaniam, R., Effect of nanocrystalline grain size on the electrochemical and corrosion behavior of nickel, *J. Corros. Sci.,* 2004, vol. 46, pp. 3019–3029.
38. Magdalena, P., Antoni, B., and Eugeniusz, Ł., Structure and corrosion resistance of nickel coatings containing tungsten and silicon powders, *J. Mater. Character.,* 2007, vol. 58, pp. 371–375.
39. Priyantha, N., Jayaweera, P., Macdonald, D.D., and Sun, A., An electrochemical impedance study of Alloy 22 in NaCl brine at elevated temperature. I. Corrosion behavior, *J. Electroanal. Chem.,* 2004, vol. 572, pp. 409–419.
40. Macdonald, D.D., Sun, A., Priyantha, N., and Jayaweera, P., An electrochemical impedance study of Alloy-22 in NaCl brine at elevated temperature: II. Reaction mechanism analysis, *J. Electroanal. Chem.,* 2004, vol. 572, pp. 421–431.
41. Li, Q., Yang, Q.X., Zhang, L., Wang, J., and Chen, B., Corrosion resistance and mechanical properties of pulse electrodeposited Ni–TiO_2 composite coating for sintered NdFeB magnet, *J. Alloys Compd.,* 2009, vol. 482, pp. 339–344.
42. Szczygieł, B. and Kolodziej, M., Composite Ni/Al_2O_3 coatings and their corrosion resistance, *J. Electrochim. Acta,* 2005, vol. 50, pp. 4188–4195.
43. Lian, J.S., Li, G.Y., Niu, L.Y., Gu, C.D., Jiang, Z.H., and Jiang, Q., Electroless Ni–P deposition plus zinc phosphate coating on AZ91D magnesium alloy, *J. Surf. Coat. Technol.,* 2006, vol. 200, pp. 5956–5962.
44. Balaraju, J.N., Ezhil Selvi, V., Willium Grips, V.K., and Rajam, K.S., Electrochemical studies on electroless ternary and quaternary Ni–P based alloys, *J. Electrochim. Acta,* 2006, vol. 52, pp. 1064–1074.
45. Abdel Aal, A., Hard and corrosion resistant nanocomposite coating for Al alloy, *J. Mater. Sci. Eng.,* 2008, vol. 474, pp. 181–187.
46. Hu, C.C. and Bai, A., Effects of annealing temperatures on the physicochemical properties of nickel-phosphorus deposits, *J. Mater. Chem. Phys.,* 2003, vol. 79, pp. 49–57.
47. Shervedani, R.K. and Lasia, A., Evaluation of the surface roughness of microporous Ni–Zn–P electrodes by in situ methods, *J. Appl. Electrochem.,* 1999, vol. 29, pp. 979–986.
48. Contreras, A., Leon, C., Jimenez, O., Sosa, E., and Perez, R., Electrochemical behavior and microstructural characterization of 1026 Ni–B coated steel, *J. Appl. Surf. Sci.,* 2006, vol. 253, pp. 592–599.
49. Shervedani, R.K., Mehrjardi, A.H., and Zamiri, N., A novel method for glucose determination based on electrochemical impedance spectroscopy using glucose oxidase self-assembled biosensor, *J. Bioelectrochem.,* 2006, vol. 69, pp. 201–208.